# Microsphere-Integrated Photonic Crystal Sensors for Spatially-Resolved Refractive Index Measurement

Jingyu Yu, Jiaming Qian, Jun Liu, Songlin Yang, Sorin Melinte, Kemao Qian, *Member, IEEE*, Chao Zuo, *Senior Member, IEEE*, and Ran Ye

***Abstract*—Refractometers based on interferometric methods require sophisticated systems and stable environment. Non-interferometric refractometers can offer advantages in terms of reducing device costs and simplifying device configurations. In this Letter, we proposed a microsphere-integrated photonic crystal (PC) refractometer with a high spatial resolution. The refractometer forms magnified patterns of the PC substrate when immersed in liquid. By invoking the two-dimensional windowed Fourier transform to analyze the patterns, the refractive index of liquid can be determined. The validity of the proposed method is verified by measuring both standard uniform liquids and the dynamic process of oil-water merging, suggesting it is a simple and effective tool for measuring RI with spatially resolved micrometer-scale resolution.**

***Index Terms*—Microsphere, refractometer, photonic crystal, photonic nanojet.**

REFRACTIVE index (RI) is one of the most important physical characteristics, offering valuable information about the composition and microstructure of the material. As a non-invasive quantitative approach, RI sensing finds extensive applications across a spectrum of disciplines, including biochemical analysis [1], environmental monitoring [2], industrial testing [3], optical metrology [4], etc. The RI of a liquid sample is usually determined by either interferometric or non-interferometric methods. Interferometric refractometers include devices based on Mach-Zehnder interferometers [5], Fabry-Perot interferometers [6], [7], and optical fiber refractometers [8]. They typically exhibit changes in their optical spectra in response to the RI fluctuations of environment. Despite the high sensitivities achievable with interferometric sensors, these devices often come with demanding requirements for both operating conditions and light sources, which significantly increases the complexity of setup.

Received 12 March 2025; revised 20 April 2025; accepted 14 June 2025. Date of publication 2 July 2025; date of current version 16 July 2025. This work was supported by the National Natural Science Foundation of China under Grant 62105156, Grant 62227818, Grant 62361136588, Grant 62305162, and Grant U21B2033. *(Jingyu Yu and Jiaming Qian contributed equally to this work.) (Corresponding author: Ran Ye.)*

Jingyu Yu, Jun Liu, Songlin Yang, and Ran Ye are with the School of Computer and Electronic Information, Nanjing Normal University, Nanjing 210023, China (e-mail: ran.ye@njnu.edu.cn).

Jiaming Qian and Chao Zuo are with the Smart Computational Imaging Laboratory (SCILab), School of Electronic and Optical Engineering, Nanjing University of Science and Technology, Nanjing 210094, China.

Sorin Melinte is with the Institute of Information and Communication Technologies, Electronics and Applied Mathematics, Université catholique de Louvain, 1348 Ottignies-Louvain-la-Neuve, Belgium.

Kemao Qian is with the School of Computer Science and Engineering, Nanyang Technological University, Singapore 639798.

Color versions of one or more figures in this letter are available at https://doi.org/10.1109/LPT.2025.3585430.

Compared with interferometric methods, non-interferometric methods have the advantages of reducing the device cost and simplifying the device configuration. For example, the RI of liquid can be determined by measuring the optical transmittance of a waveguide [9] or 3D cascade microlens groups [10]. Yoon and Yang found that the change of liquid RI leads to a defocus in image systems. The RI of liquid can be determined by analyzing this defocus [11]. Recently, microfluidic channels patterned with diffraction gratings have been successfully used for RI sensing of small liquid flow, in which the intensity of the first-order diffraction of the grating can be significantly affected by the RI of sample liquid [12], [13].

Among various non-interferometric methods, photonic crystal (PC) sensors have attracted great attention because they can be performed on-spot for rapid inspection simply by the observation of naked eyes [14]. PCs are ordered structures created by periodically arranging two or more substances with different RI. They show brilliant colors under white light illumination due to the coherent scattering of light by their periodic structures. For this reason, they have been successfully used as colorimetric sensors to measure various physical and chemical parameters, including mechanical deformation [15], pH value of liquid [16], and to distinguish organic compounds [17]. When a PC sensor responds to external stimuli, there will be a change in the lattice spacing of its structure, or in its average effective RI. This change causes shift of diffractive peaks in its spectrum, and consequently leads to a change of its color. However, the PC sensors have a low spatial resolution because reducing the sensing area will weaken the effects of coherent scattering and the optical response of the sensor.

In this Letter, we present a multifunctional refractometer for measuring the refractive index (RI) of liquids. The device consists of a stripe-patterned photonic crystal (PC) substrate with a layer of microsphere (MS) lenses on top [Fig. 1(a)]. The stripe pattern enables a colorimetric response to RI changes, similar to conventional PC sensors. Additionally, the microlenses produce magnified images of the underlying pattern. Because the magnification ability of the microlens is dependent on the liquid RI, the spatial frequency of the magnified pattern changes with the RI of liquid, as illustrated in Fig. 1(b). By invoking the two-dimensional windowed Fourier transform to analyze the stripe patterns, the ridge of the local Fourier spectrum (so-called spectrogram) can be extracted, from which we can determine the RI of liquid. The spatial distribution of the RI over the whole field-of-view (FOV) can be measured in this way by using monolayers of microlens arrays to fully cover the patterned substrate.

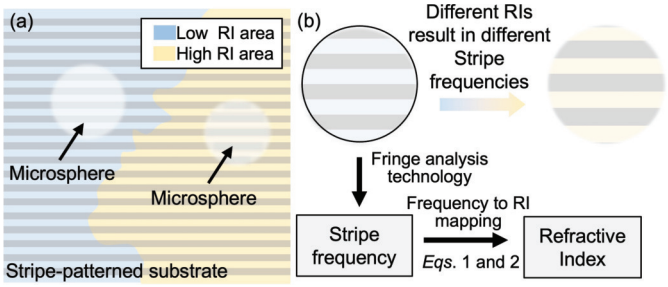


Fig. 1. Flowchart of spatially-resolved RI measurement using the proposed refractometers. (a) Microspheres distributed in liquids of different RIs on stripe-patterned substrates; (b) Process of obtaining RI using fringe analysis.

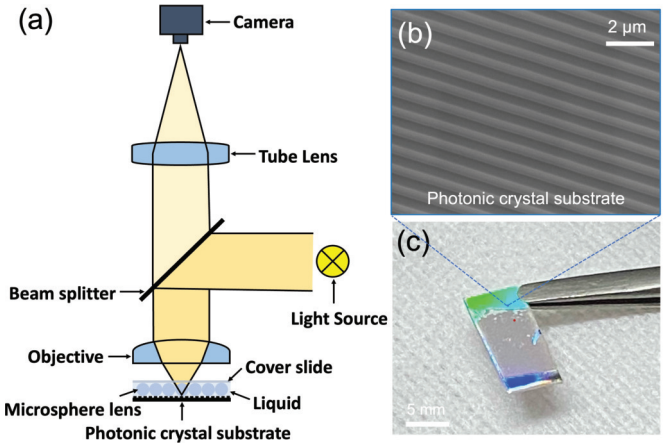


Fig. 2. (a) Schematic drawing of the RI measurement platform; (b) Scanning electron microscopic (SEM) image of the substrate; (c) Optical microscopic image of the refractometer.

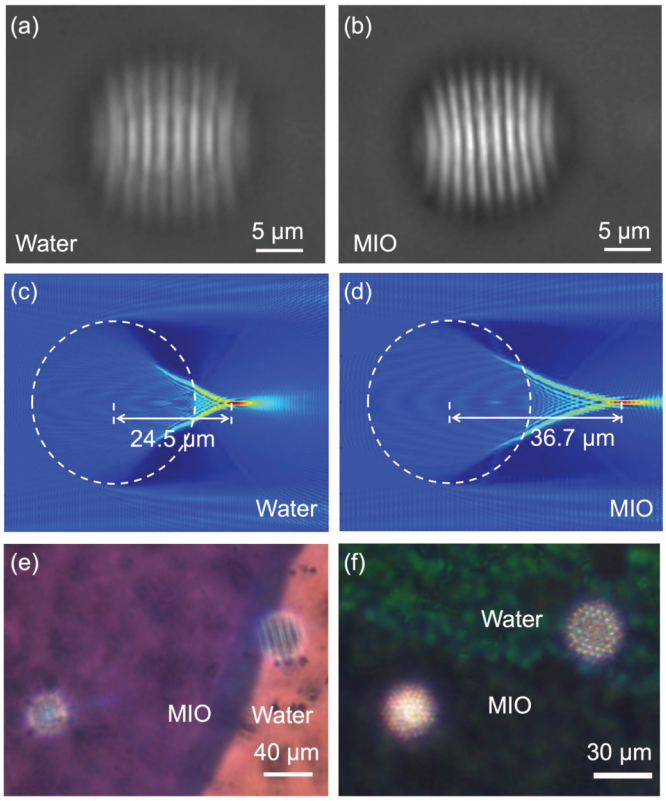


Fig. 3. (a), (b) Magnified stripe patterns of the refractometer (a) in water and (b) in MIO; (c), (d) Simulated focal length of the microsphere (c) in water and (d) in MIO; (e), (f) Spatially-resolved RI measurement of a water-MIO film using the refractometer with (e) a stripe pattern and (f) a hexagonally-close-packed (hcp) pattern.

The platform for RI measurement is shown in Fig. 2(a). The refractometer has a sandwiched structure composed of a coverslide, a monolayer of microlens arrays and a patterned substrate, and it was observed under a conventional optical microscope (Axio AX10, Carl Zeiss) under white light illumination (HAL 100, Carl Zeiss). The pattern of the substrate is magnified first by the microlens, and then a 50× objective (NA =0.75, EPIPLAN, Carl Zeiss). A digital camera (DFC295, Leica) was used to capture the optical microscopic images.

Two types of microlenses were employed in this study to demonstrate the versatility of this method. The first type is barium titanate glass (BTG, n =1.90) microspheres. They were provided by the Microspheres-Nanospheres, USA as powders with a mean diameter of ~ 35 $\mu$m [Fig. S1(a)]. The second type is 4.9 $\mu$m-diameter polystyrene (PS, n =1.59) microspheres [Fig. S1(b)] purchased from Microparticles, German as colloidal suspensions. Before experiments, BTG microspheres and PS microspheres were put onto PC substrates as centimeter-sized monolayers of microlens arrays by drop-casting [Fig. S2] and self-assembly [Fig. S3], respectively.

As an initial demonstration, we used DVD discs as the substrate, which have a stripe pattern with a periodicity of 0.75 $\mu$m [Fig. 2(b)]. The disc shows brilliant color under white light illumination due to the coherent scattering of periodic structures [Fig. 2(c)]. The gray area on the disc is a film of microsphere arrays.

Then, we used the refractometer to visualize the RI difference between water (n =1.33) and microscope immersion oil (MIO, n =1.52). Figs. 3(a) and 3(b) show the stripe pattern imaged by BTG microspheres (D = 35 $\mu$m). The magnification factor of the pattern is 3.2× in water and 2.9× in MIO, respectively. This difference in magnification factors is due to the difference in the focal length of microspheres. To show the light focusing properties of microspheres in the two liquids, we performed simulations with the Finite-Difference Time-Domain (FDTD) method. For the entire computational domain, non-uniform meshes with refractive index-dependent element size were used and all of them are smaller than $\lambda$/50. The perfectly matched layer (PML) was set as the boundary condition of the simulation domain to absorb incident light with minimal reflections. As shown in Figs. 3(c) and 3(d), the focal length, referring to the distance between the focal point and the center of the microsphere, is 24.5 $\mu$m in MIO and 36.7 $\mu$m in water. Since an optical lens with a longer focal length generally has a smaller magnification ability, changes in liquid RI will immediately affect the magnification of the stripe pattern.

To demonstrate the spatially resolved RI measurement capability of the refractometer, we drop-casted water and MIO on a MS-PC refractometer. As shown in Fig. 3(e), the stripe patterns have different magnification factors in these two liquids, and the refractometer shows purple in MIO and light brown in water. According to the Bragg diffraction theory, the resonance wavelength of a PC is determined by its period ($\Lambda$) of grating and its effective RI ($n_{eff}$), which can be described with the equation of $\lambda_{resonance} = n_{eff}\Lambda$ [18]. The effective RI here is considered as a weighted average of the RI of the materials

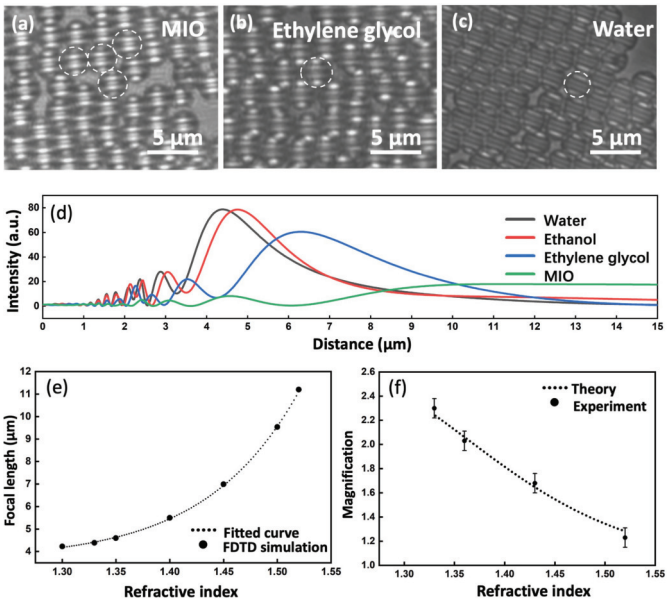


Fig. 4. (a)-(c) Refractometers with 4.9 $\mu$m-diameter PS microsphere lenses in (a) MIO, (b) ethylene glycol and (c) water; (d) Simulated intensity profiles along the optical axis of the microsphere; (e) Simulated focal length of the microsphere as a function of liquid RI; (f) Theoretical and experimental magnification factor of the microsphere at different liquid RI.

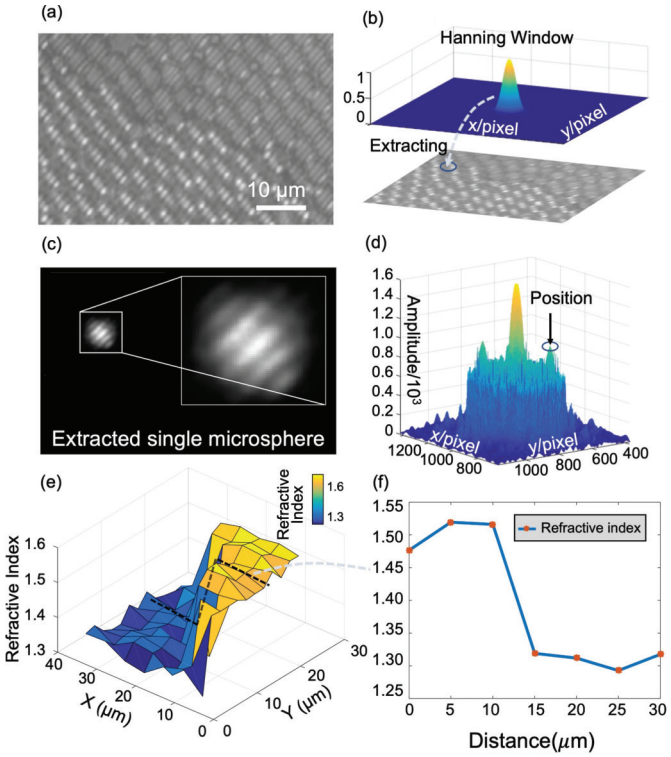


Fig. 5. (a) Optical microscopic image of water (left) and MIO (right) films on a MS-PC refractometer; (b) Extraction of single microsphere using Hanning window; (c) Extracted stripe pattern magnified by an individual microsphere; (d) Fourier spectrum map of (c); (e) Map of the RI distribution of (a). (f) RI distribution of the dotted line in (e).

in which the resonant mode is supported [19]. At a constant $\Lambda$, the $\lambda_{resonance}$ increases with the $n_{eff}$. In our measurement, the sample liquids change the $n_{eff}$ of the refractometer and induce a shift of $\lambda_{resonance}$ in the reflection spectrum of the refractometer. The proposed refractometer is also compatible with substrates of different structures and materials. Figure 3(f) presents an example of RI measurement using a refractometer with a substrate composed of hexagonally close-packed (hcp) silica particle arrays with a diameter of $\sim$ 900 nm.

Next, we used refractometers with 4.9 $\mu$m-diameter PS microspheres placed on top of the stripe pattern to perform refractive index measurements with higher spatial resolution. As shown in Figs. 4(a)-(c), the microspheres were arranged into hcp arrays by the self-assembly method [20], [21]. A green interference filter (central wavelength $\lambda$ = 550 nm, 45 nm bandwidth) was used to reduce the chromatic aberration of the microlens, and the obtained images were converted into grayscale mode. The white circles in Figs. 4(a)-(c) indicate that each microsphere works as an individual lens to magnify the pattern underneath. The stripe pattern has a magnification factor of 2.32×, 2.04×, 1.65× and 1.21× in water, ethanol, ethylene glycol, and MIO, respectively. It is possible to make PS microspheres cover the whole FOV of the microscope, enabling the MS-PC sensors to perform whole-field sensing by analyzing the magnified fringe patterns using the windowed Fourier ridges [22], [23]. However, defects such as the dimensional deviation of microspheres and the misalignment of PC structures will affect measurement accuracy by changing the frequency of the stripe pattern. Apart from using high-quality devices, we can also enhance the accuracy by collecting data from multiple microspheres immersed in the same liquid of interest and averaging the results.

To study the correlation between the RI of liquid and the magnification factor of the PS microspheres, we simulated the focal length of PS microspheres with the FDTD method. Figure 4(d) shows the intensity profiles along the axis of the microspheres immersed in water, ethanol, ethylene glycol and MIO. The intensity increases from the edge of the microsphere until to the focal point, and then it gradually decreases to zero. The region of the maximum intensity is considered as the focal point. Equation 1 is obtained by fitting the simulated focal length obtained at different RI of liquid, where $f_{MS}$ is the focal length of the microsphere, $n_{liquid}$ is the RI of liquid. As shown in Fig. 4(e), Eq. 1 satisfactorily fits the FDTD result.

$$f_{MS} = 4.797 \cdot e^{-0.2346 \cdot n_{liquid}} + 2.732 \cdot 10^{-7} \cdot e^{11.29 \cdot n_{liquid}} \quad (1)$$

The magnification factor of a lens can be calculated using Eq. 2, where $l$ is the distance between the pattern and the center of the microsphere. As shown in Fig. 4(f), the experimental values of magnification factor as a function of the liquid RI are close to the theoretical ones given by the Eq. 2.

$$M_{MS} = \frac{f_{MS}}{f_{MS} - l} \quad (2)$$

Then, we simultaneously applied small amount of water and MIO onto the left and right part of a MS-PC refractometer and performed spatially resolved RI measurement. As shown in Fig. 5(a), the boundary between water and MIO films can be easily seen with the help of the PC substrate. As shown in Figs. 5(b) to 5(f), then we quantify the spatially varying RI/frequencies using the 2D windowed Fourier ridges algorithm [22], [23]. Specifically, each microsphere is extracted by a Hanning window centered at $\mathbf{r}_0$ (the size of the window

function depends on the microsphere size) [Eq. 3, Figs. 5(b) and 5(c)]:

$$D(\mathbf{r}) \approx \begin{cases} [A + m\cos(2\pi\mathbf{k}_e\mathbf{r} + \varphi) + n(\mathbf{r})] \cdot H(\mathbf{r}) & H(\mathbf{r}) > 0 \\ 0 & H(\mathbf{r}) = 0 \end{cases} \tag{3}$$

where $D$ represents the processed image which can be approximated as a sine function in the effective region, $\mathbf{r}$ denotes the spatial coordinate, $H$ is the Hanning window, $A$ and $m$ are the average intensity and modulation, respectively, which are assumed constants, $\mathbf{k}_e$ denotes the spatial frequency of the fringes, $\varphi$ is the phase (also assumed to be constant), and $n$ represents the random noise. Then its spectrum information in the effective region is obtained by the Fourier transform (Eq. 4):

$$\tilde{D}(\mathbf{k}) = 2\pi A\delta(\mathbf{k}) + \frac{m}{2}\delta(\mathbf{k} + \mathbf{k}_e)e^{-j\varphi} + \frac{m}{2}\delta(\mathbf{k} - \mathbf{k}_e)e^{j\varphi} + \tilde{n}(\mathbf{k}) \tag{4}$$

where $\sim$ denotes the Fourier transform of the original object, $\mathbf{k}$ is the frequency coordinate, and $\delta$ represents the unit pulse function. Since the sinusoidal components are much larger than other components such as noise, we can directly position the first-order spectral center to obtain the approximate spatial frequency $\mathbf{k}_e$ at $\mathbf{r}_0$ point [Fig. 5(d)], followed by obtaining the RI through the relationship between frequency and RI [Eqs. 1 and 2]. The RI distribution of the whole image is achieved by performing the above steps for the region where each microsphere is located [Figs. 5(e) and 5(f)]. The real-time dynamic RI measurement of the water-MIO hybrid films is shown in Visualization 1, in which the boundary between the two liquids kept moving.

In conclusion, a new type of refractometer has been developed in this work. The refractometer comprises microsphere lenses and a patterned substrate. During RI measurement, each microsphere forms a magnified image of the substrate patterns below, with a magnification factor dependent on the RI of sample liquid. By extracting the spectrogram for each microsphere with the 2D windowed Fourier transform, the RI spatial distribution over the whole FOV can be effectively determined based on the frequency of the patterns. The developed refractometer has a good compatibility with commercial optical microscopes, and can be used as a label-free, point-of-care device for rapid detection of various liquids.

## REFERENCES


[1] C. Peng et al., "Optical waveguide refractive index sensor for biochemical sensing," *Appl. Sci.*, vol. 13, no. 6, p. 3829, Mar. 2023.

[2] J. Chen, W. Guo, M. Xia, W. Li, and K. Yang, "In situ measurement of seawater salinity with an optical refractometer based on total internal reflection method," *Opt. Exp.*, vol. 26, no. 20, pp. 25510–25523, 2018.

[3] A. Seki, K. Narita, and K. Watanabe, "Refractive index measurement in sucrose solution and beverage using surface plasmon resonance sensor based on hetero-core structured fiber optic," *Proc. Chem.*, vol. 20, pp. 115–117, Jan. 2016.

[4] C. Zuo et al., "Deep learning in optical metrology: A review," *Light, Sci. Appl.*, vol. 11, no. 1, p. 39, Feb. 2022.

[5] H. Yu et al., "Ultracompact and high sensitive refractive index sensor based on Mach–Zehnder interferometer," *Opt. Lasers Eng.*, vol. 56, pp. 50–53, May 2014.

[6] B. Xu, Y. Yang, Z. Jia, and D. N. Wang, "Hybrid Fabry–Pérot interferometer for simultaneous liquid refractive index and temperature measurement," *Opt. Exp.*, vol. 25, no. 13, p. 14483, 2017.

[7] G. Li, X. Cen, J. Su, and C. Wu, "Fabry–Pérot cavity enhanced prism for highly sensitive refractive index measurement of water," *Optik*, vol. 245, Nov. 2021, Art. no. 167688.

[8] Y. Ma et al., "Refractometer based on fiber Mach–Zehnder interferometer composed of two micro bending cores," *Opt. Exp.*, vol. 29, no. 20, pp. 31443–31454, 2021.

[9] D. Barshilia, L.-K. Chau, and G.-E. Chang, "Low-cost planar waveguide-based optofluidic sensor for real-time refractive index sensing," *Opt. Exp.*, vol. 28, no. 19, pp. 27337–27345, 2020.

[10] J. Tang, G. Qiu, X. Zhang, and J. Wang, "A 3D-cascade-microlens optofluidic chip for refractometry with adjustable sensitivity," *Lab Chip*, vol. 21, no. 19, pp. 3784–3792, Sep. 2021.

[11] S. Y. Yoon and S. Yang, "Microfluidic refractometer with micro-imaging defocusing," *Lab Chip*, vol. 11, p. 8512, Mar. 2011.

[12] F. Purr, M. Bassu, R. D. Lowe, B. Thürmann, A. Dietzel, and T. P. Burg, "Asymmetric nanofluidic grating detector for differential refractive index measurement and biosensing," *Lab Chip*, vol. 17, no. 24, pp. 4265–4272, 2017.

[13] S. Calixto et al., "Liquid refractive index measured through a refractometer based on diffraction gratings," *Opt. Exp.*, vol. 27, no. 24, pp. 34705–34720, 2019.

[14] H. Li, J. Wang, L. Yang, and Y. Song, "Superoleophilic and superhydrophobic inverse opals for oil sensors," *Adv. Funct. Mater.*, vol. 18, no. 20, pp. 3258–3264, Oct. 2008.

[15] P. Escudero, J. Yeste, C. Pascual-Izarra, R. Villa, and M. Alvarez, "Color tunable pressure sensors based on polymer nanostructured membranes for optofluidic applications," *Sci. Rep.*, vol. 9, no. 1, p. 3259, Mar. 2019.

[16] J. Shin, P. V. Braun, and W. Lee, "Fast response photonic crystal pH sensor based on templated photo-polymerized hydrogel inverse opal," *Sens. Actuators B, Chem.*, vol. 150, no. 1, pp. 183–190, Sep. 2010.

[17] T. Endo, Y. Yanagida, and T. Hatsuzawa, "Colorimetric detection of volatile organic compounds using a colloidal crystal-based chemical sensor for environmental applications," *Sens. Actuators B, Chem.*, vol. 125, no. 2, pp. 589–595, Aug. 2007.

[18] H. Inan et al., "Photonic crystals: Emerging biosensors and their promise for point-of-care applications," *Chem. Soc. Rev.*, vol. 46, no. 2, pp. 366–388, Jan. 2017.

[19] I. D. Block, N. Ganesh, M. Lu, and B. T. Cunningham, "A sensitivity model for predicting photonic crystal biosensor performance," *IEEE Sensors J.*, vol. 8, no. 3, pp. 274–280, Mar. 2008.

[20] R. Ye, Y.-H. Ye, Z. Zhou, and H. Xu, "Gravity-assisted convective assembly of centimeter-sized uniform two-dimensional colloidal crystals," *Langmuir*, vol. 29, no. 6, pp. 1796–1801, Feb. 2013.

[21] F. Cheng, S. Yang, X. Wang, P. He, R. Ye, and Y. Ye, "Fabrication of two-dimensional silica colloidal crystals via a gravity-assisted confined self-assembly method," *Colloids Interface Sci. Commun.*, vol. 37, Jun. 2020, Art. no. 100286.

[22] Q. Kemao, "Windowed Fourier transform for fringe pattern analysis," *Appl. Opt.*, vol. 43, no. 13, pp. 2695–2702, 2004.

[23] Q. Kemao, H. Wang, and W. Gao, "Windowed Fourier transform for fringe pattern analysis: Theoretical analyses," *Appl. Opt.*, vol. 47, no. 29, pp. 5408–5419, 2008.